Journal of Colloid and Interface Science 676 (2024) 101–109

Contents lists available at ScienceDirect

Journal of Colloid And Interface Science

journal homepage: www.elsevier.com/locate/jcis

Regular Article

Enhancing tumor endothelial permeability using MUC18-targeted gold nanorods and mild hyperthermia

Xiao Yu [a], Jinyuan Liu [a], Aaron Bauer [a], Xianqing Wei [b], Steve Smith [a], Shipeng Ning [b,*], Congzhou Wang [a,*]

[a] Nanoscience and Biomedical Engineering, South Dakota School of Mines and Technology, 501 E St Joseph Street, Rapid City, South Dakota 57701, USA
[b] Department of Breast Surgery, The Second Affiliated Hospital of Guangxi Medical University, Nanning, China

GRAPHICAL ABSTRACT

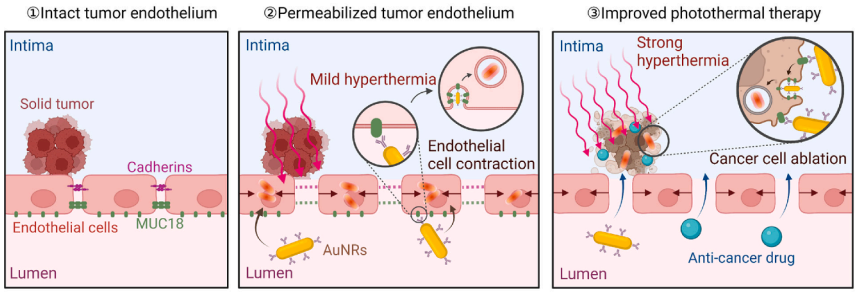

ARTICLE INFO

Keywords:
Tumor endothelial permeability
MUC18
Gold nanorods
Mild hyperthermia
Cancer therapy

ABSTRACT

The Enhanced Permeability and Retention (EPR) effect, an elevated accumulation of drugs and nanoparticles in tumors versus in normal tissues, is a widely used concept in the field of cancer therapy. It assumes that the vasculature of solid tumors would possess abnormal, leaky endothelial cell barriers, allowing easy access of intravenous-delivered drugs and nanoparticles to tumor regions. However, the EPR effect is not always effective owing to the heterogeneity of tumor endothelium over time, location, and species. Herein, we introduce a unique nanoparticle-based approach, using MUC18-targeted gold nanorods coupled with mild hyperthermia, to specifically enhance tumor endothelial permeability. This improves the efficacy of traditional cancer therapy including photothermal therapy and anticancer drug delivery by increasing the transport of photo-absorbers and drugs across the tumor endothelium. Using single cell imaging tools and classic analytical approaches in molecular biology, we demonstrate that MUC18-targeted gold nanorods and mild hyperthermia enlarge the intercellular gaps of tumor endothelium by inducing circumferential actin remodeling, stress fiber formation, and cell contraction of adjacent endothelial cells. Considering MUC18 is overexpressed on a variety of tumor endothelium and cancer cells, this approach paves a new avenue to improve the efficacy of cancer therapy by actively enhancing the tumor endothelial permeability.

* Corresponding authors.
E-mail addresses: nspdoctor@sr.gxmu.edu.cn (S. Ning), congzhou.wang@sdsmt.edu (C. Wang).

https://doi.org/10.1016/j.jcis.2024.07.047
Received 14 May 2024; Received in revised form 13 June 2024; Accepted 5 July 2024
Available online 14 July 2024

1. Introduction

Cancer therapy depends heavily on the Enhanced Permeability and Retention (EPR) effect, an important concept assuming a preferred accumulation of intravenous-delivered anticancer drugs and nanoparticles in tumors versus normal organs.[1–3] This is because the vasculature of solid tumors typically possesses abnormal, leaky endothelial cell barriers due to the enlarged inter-endothelial cell gaps, promoting the access of blood-circulating substances to the tumor regions.[4–6] However, recent studies indicate the EPR effect is not always effective owing to the heterogeneity of tumor endothelium over time and location.[7,8] For instance, the leaky vasculature needed for the EPR effect is mainly observed in the late-stage instead of early-stage tumors, although treating the early-stage tumors should be simpler and pursued.[9] In terms of tumor origins, some tumors (e.g., pancreatic cancer) exhibit non-leaky blood vessels with a well-structured, intact endothelium that hinders the use of EPR effect for drug and nanoparticle delivery.[10] Apart from temporal and spatial variations, recent studies show that the EPR effect is also species-dependent: most EPR effects were demonstrated in mouse models, but less prominent in tumors from human patients, which accounted for some failed clinical trials.[11] Based on these considerations, developing strategies to increase endothelial permeability will significantly boost the efficacy of targeted drug and nanoparticle delivery, and further advance the field of cancer therapy.

Intentionally enhancing endothelial permeability using physical and biochemical stimuli can be a route to overcome the challenges posed by an insufficient EPR effect. These stimuli, including heat, ultrasound, radiotherapy, pharmacological agents, and nanoparticles, are able to increase endothelial permeability through different mechanisms and thus enhance the EPR effect for drug and nanoparticle delivery.[12–16] Unfortunately, most of these approaches suffer from off-target effects and damage to healthy tissues, limiting their practical application.[7] To address this issue, researchers have proposed to use local hyperthermia produced by plasmonic gold nanorods and near-infrared laser irradiation to enlarge the gap size and increase the permeability of tumor endothelium.[17,18] While this approach is effective in preventing off-target effect, the local modulation of endothelial permeability still relies on the accumulation of a sufficient amount of gold nanorods via pre-existing EPR effect to reach elevated temperature upon laser irradiation. Typically, gold nanorods are functionalized with non-targeted polyethylene glycol (PEG) to extend their circulation time and maximize the EPR effect (if it exists). However, the EPR effect may not be sufficient to allow the accumulation of enough gold nanorods, which compromises the feasibility of these approaches. Strategies to directly target tumor endothelial cells and induce tumor endothelial permeability should improve drug and nanoparticle accumulation in tumor regions, while minimizing the adverse effects on other parts of the body.

MUC18, also known as CD146, is a transmembrane protein over expressed on a variety of tumor endothelium, and its expression level on tumor endothelial cells typically upregulates 2 to 4 fold compared to normal endothelial cells.[19] It was found that MUC18 is homogenously distributed on almost all tumor vessels, and its expression level is independent of tumor size and maturity.[20] The elevated level of MUC18 was demonstrated to promote tumor angiogenesis and maintain cell–cell adhesion of tumor endothelial cells.[21] Hence, MUC18 not only serves as an excellent tumor endothelial marker, but also contributes to the regulation of tumor endothelial permeability. Besides tumor endothelium, MUC18 is also a well-established cell adhesion molecule, which is overexpressed on many cancer cells including melanoma, breast cancer, and prostate cancer.[22] Inspired by these findings, this study introduces MUC18-targeted gold nanorods, combined with mild hyperthermia induced by near-infrared laser irradiation, to specifically enhance tumor endothelial permeability and improve the efficacy of traditional photothermal therapy and anticancer drug delivery (Fig. 1). Considering the multifaceted roles of MUC18, the MUC18-targeted gold nanorods here are expected to exert multiple functions: (a) targeting tumor endothelial cells; (b) disrupting the downstream signaling of MUC18 to enhance tumor endothelial cell contraction and EPR effects; and (c) targeting MUC18-positive cancer cells to improve the efficacy of photothermal ablation of cancer cells. Overall, this approach offers a new opportunity to improve the efficacy of cancer therapy (i.e., chemotherapy, photothermal therapy) by actively and specifically inducing the EPR effect in tumor endothelium.

2. Results and discussion

2.1. Functionalization and characterization of gold nanorods

Gold nanorods (AuNRs) were synthesized using a seed-mediated method, which involves the initial formation of seed nanospheres and subsequent anisotropic growth to nanorods in the presence of cetyltrimethylammonium bromide (CTAB), a cationic capping agent.[23–25] To prepare MUC18-targeted AuNRs, the CTAB-capped AuNRs first underwent a ligand exchange process to displace the CTAB with a protein layer consisting of streptavidin (str) and bovine serum albumin (BSA), followed by the surface conjugation with biotinylated anti-MUC18 antibody via the strong binding affinity between streptavidin and biotin (Fig. 2A). This design offers multiple advantages: (i) The cytotoxic CTAB can be completely removed during the ligand exchange process; [26,27] (ii) Streptavidin, a tetrameric protein with four biotin-binding

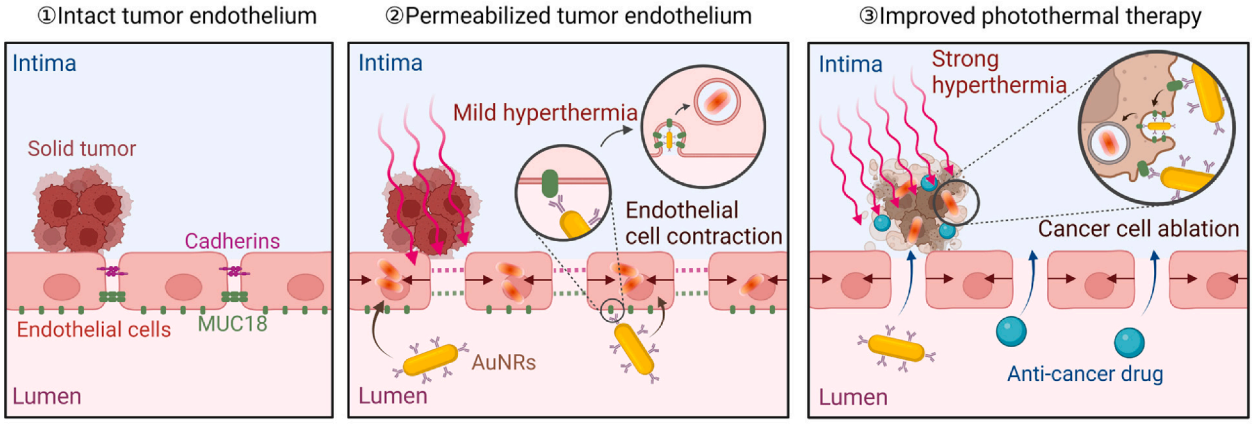

Fig. 1. Overall concept of this work: MUC18-targeted AuNRs and mild hyperthermia are used to enhance the tumor endothelial permeability and efficacy of photothermal therapy and anticancer drug delivery.

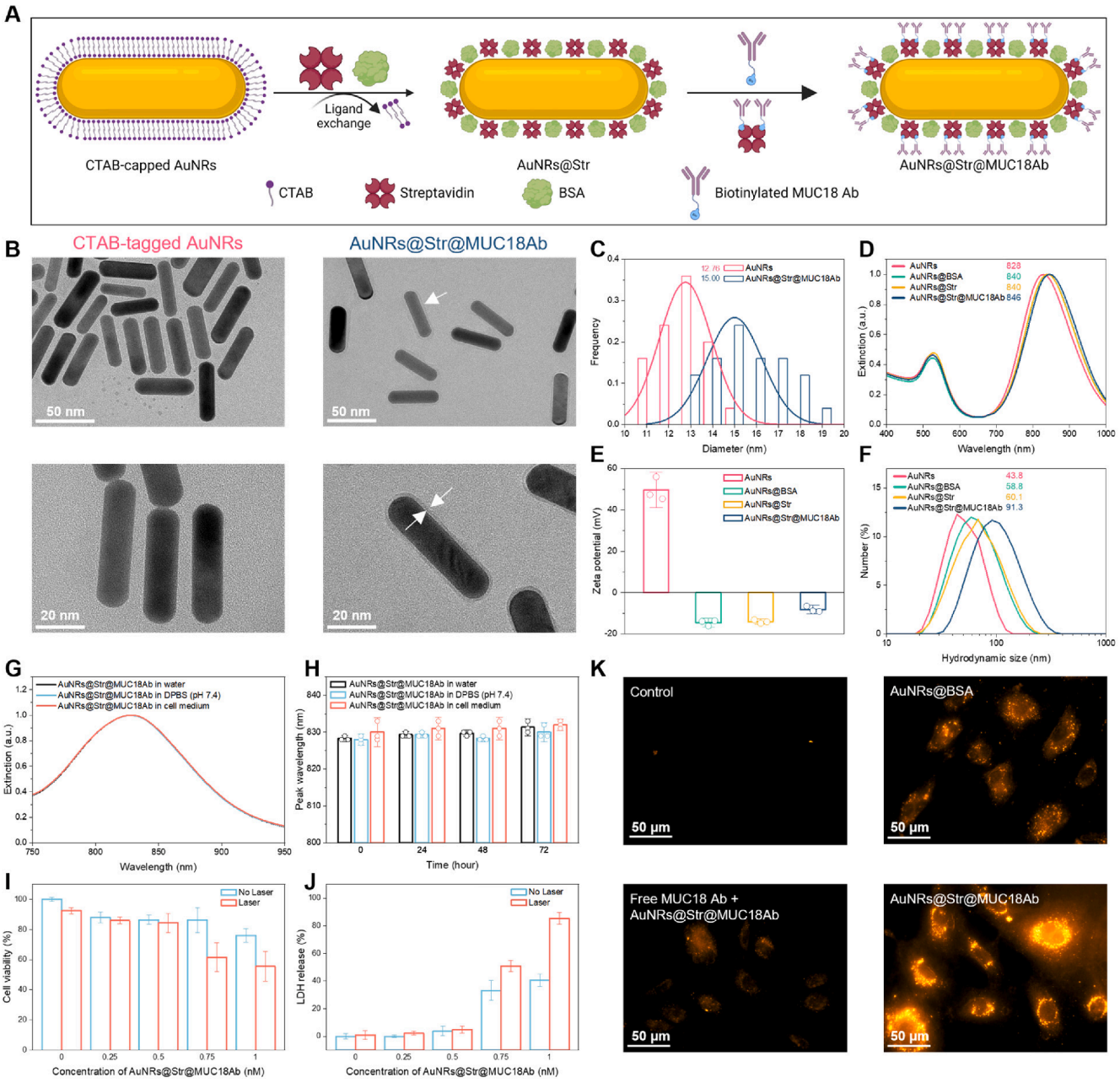

Fig. 2. Functionalization, characterization, cytotoxicity, and endothelial-targeting ability of AuNRs. (A) Schematic illustrating the antibody functionalization steps on AuNRs. (B) TEM images of CTAB-capped AuNRs and MUC18 antibody functionalized AuNRs. The white arrows mark the protein coating around nanorod surface. (C) Statistical analysis of nanorod diameter increase from TEM images. (D) Extinction spectra, (E) zeta potential, and (F) hydrodynamic size of AuNRs with different surface functionalization. (G) Extinction spectra of MUC18 antibody functionalized AuNRs in different media. (H) LSPR peak wavelength of MUC18 antibody functionalized AuNRs in different media for 72 h. Data are mean ± SD, n = 3. (I) Cell viability and (J) LDH release of HUVEC when subjected to different treatments. Data are mean ± SD, n = 5. (K) Darkfield images of HUVEC before and after incubation with different groups of AuNRs.

sites, can strongly conjugate biotinylated antibody and prevent direct contact of antibody with nanorod surface which may cause antibody deactivation;[28] and (iii) BSA, functioning as a spacer, can be used to adjust the antibody density on the nanorod surface, avoiding the crowding effect while minimizing the nonspecific binding of serum proteins and the formation of protein corona.[29,30].

Transmission electron microscope images clearly show the presence of protein coating around AuNRs after antibody functionalization (Fig. 2B), and the increased diameter and length of antibody coated AuNRs from image analysis further support the visual observation (Fig. 2C and S1). UV–vis spectroscopy verified the colloid stability and near-infrared absorbance of nanorods after the stepwise surface functionalization (Fig. 2D): Upon substituting CTAB with BSA/streptavidin layer, the longitudinal localized surface plasmon resonance (LSPR) peak of AuNRs exhibited a 12 nm redshift (from 828 to 840 nm). Meanwhile, BSA-coated AuNRs (AuNRs@BSA), nontargeted nanorods with a neat BSA coating, displayed a consistent redshift of 12 nm in the LSPR peak (from 828 to 840 nm) owing to the comparable size of BSA (Mw: 57 kDa) and streptavidin (Mw: 58 kDa). Following the incubation with antibody solution, the LSPR peak of AuNRs@Str further shifted to a longer wavelength (from 840 to 846 nm), suggesting the excellent colloid stability and near-infrared absorbance of surface functionalized nanorods. Apart from imaging and spectroscopy, zeta potential and dynamic light scattering measurements also demonstrated the stepwise

functionalization of the nanorod surface (Fig. 2E-2F): As noted, the hydrodynamic size of nanorods (referring to the length of nanorods) progressively increased from 42.8 to 60.1 and finally to 91.3 nm, corresponding to the CTAB-capped AuNRs, AuNRs@Str, and AuNRs@Str@MUC18Ab, respectively. Finally, the colloidal stability of AuNRs@Str@MUC18Ab (abbreviated as AuNRs@MUC18Ab hereafter) in different aqueous solutions was confirmed by the unchanged LSPR spectra within 72 h (Fig. 2G-2H). Together, these data suggest the successful functionalization of AuNRs using MUC18 antibody and the excellent colloidal stability of the as-prepared AuNRs@MUC18Ab.

2.2. *Endothelial cytotoxicity and targeting ability of AuNRs*

Human umbilical vein endothelial cells (HUVEC) were employed as a surrogate for tumor endothelial cells because of their similar angiogenic behavior with tumor endothelial cells and the abundance of MUC18 on the HUVEC surface (**Figure S2**).[31,32] Since the ultimate goal is to enhance the tumor endothelial permeability temporarily by inducing recoverable intercellular gaps, it is important to ensure the treatments involving AuNRs@MUC18Ab and near-infrared laser exposure have a minimal cytotoxic effect on endothelial cells. Thus, we employed two classic cytotoxicity assays to quantify the mitochondrial succinate dehydrogenase (an indicator of cell viability, XTT assay) and the release of lactate dehydrogenase (a measure of membrane damage, LDH assay). The assay results suggested that lower concentrations of AuNRs@MUC18Ab (≤0.5 nM), with or without a near-infrared laser treatment (808 nm, 5 min, 0.5 W/cm^2), had negligible effects on cell viability and membrane structure, which set the stage for subsequent experiments. It should be noted that we chose the laser intensity of 0.5 W/cm^2 because: (i) it is close to the maximal permissible exposure intensity (0.3–0.4 W/cm^2) suggested by the American National Standards Institute, leading to a mild hyperthermia effect that avoids skin damage and scar formation; [28,33] and (ii) From a practical perspective, the slightly higher laser intensity here ensures the temperature increase within a short period of time (5 min).[34,35] Interestingly, the mild hyperthermia treatment has been previously applied to cancer-associated fibroblasts and cancer stem cells,[36–39] whereas the application of this treatment on endothelial cells is still lacking.

Following the identification of non-cytotoxic doses, the targeting ability of AuNRs was evaluated by dark-field microscopy. This is based on the phenomenon that AuNRs with anisotropic shape can scatter light off their surface at different angles, which offers a direct way to observe the intracellular amount and distribution of AuNRs.[40] As shown in Fig. 2K and S3-S4, HUVEC exhibited stronger light scattering after incubation with AuNRs@MUC18Ab, as compared to non-targeted AuNRs@BSA, suggesting the higher endothelial uptake and better targeting ability of AuNRs@MUC18Ab. Notably, a "ring-like" pattern around the cell nucleus indicated the intracellular localization of AuNRs@MUC18Ab after internalization. As a control experiment, HUVEC pre-treated with free MUC18 antibody reduced the cell uptake of AuNRs@MUC18Ab, further validating the specific targeting of AuNRs@MUC18Ab to MUC18 on HUVEC surface. Together, these results suggest the excellent biocompatibility and MUC18 targeting ability of AuNRs@MUC18Ab.

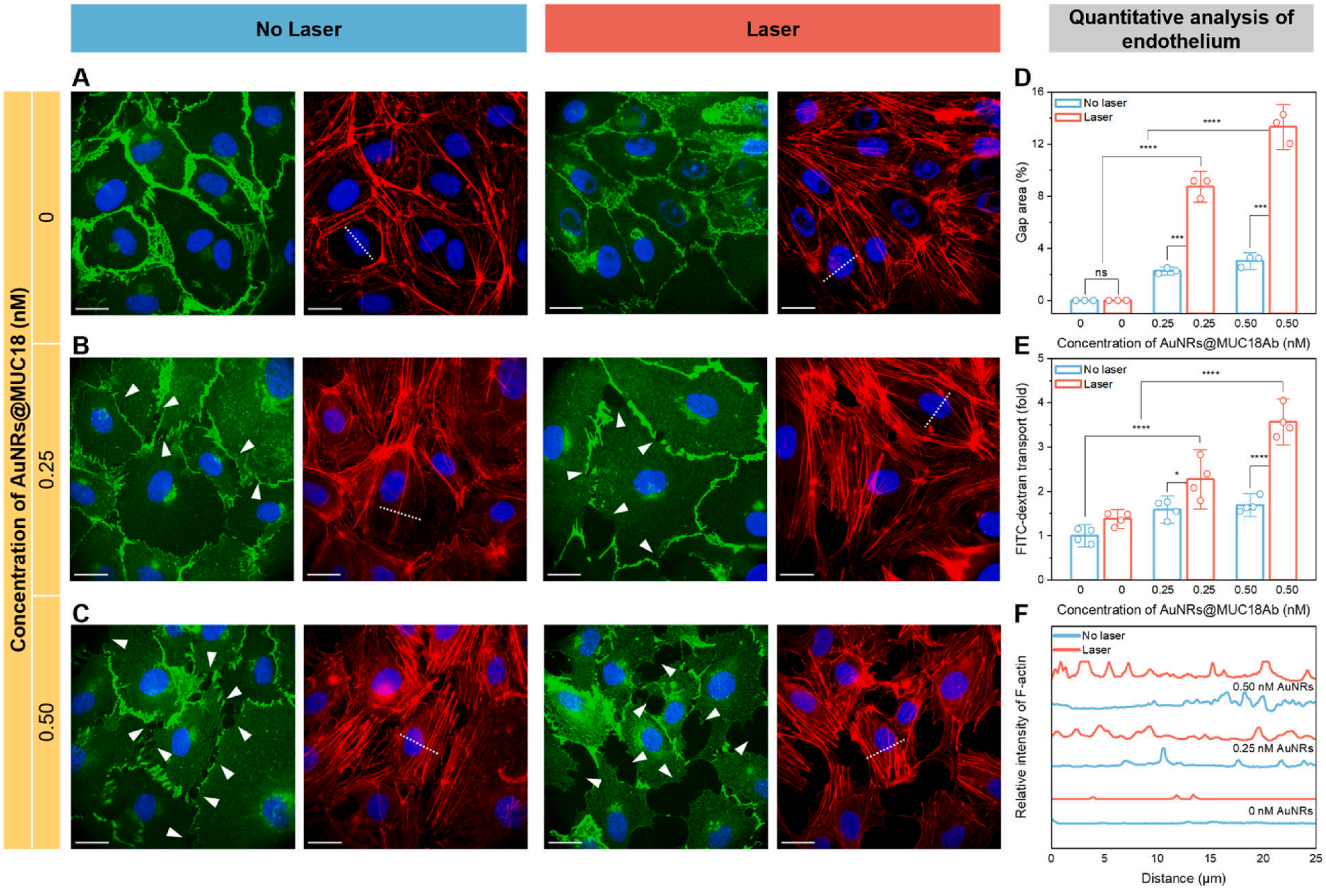

Fig. 3. AuNRs@MUC18Ab and mild hyperthermia enhance endothelial permeability. (A-C) Co-fluorescence staining of VE-cadherin (green) and F-actin (red) on HUVEC monolayers in different treatment groups. (D) Quantification of gap area on HUVEC monolayers in different treatment groups. Data are mean ± SD, n = 3. One-way ANOVA with Tukey's post-hoc tests, ***P < 0.001, ****P < 0.0001. (E) FITC-dextran transport across HUVEC monolayers in different treatment groups. The data of treated groups was normalized to the untreated group. Data are mean ± SD, n = 4. One-way ANOVA with Tukey's post-hoc tests, *P < 0.1, ****P < 0.0001. (F) F-actin intensity profiles along the white dotted lines on the fluorescence images.

2.3. AuNRs@MUC18Ab and mild hyperthermia enhance endothelial permeability

Next, we evaluated whether AuNRs@MUC18Ab and mild hyperthermia treatments affect the endothelial permeability. HUVEC was first cultured to a 100 %-confluent monolayer to mimic non-leaky tumor endothelium and then subjected to different treatments. As shown in Fig. 3A and S5, corelated fluorescence staining of VE-Cadherin and F-actin on untreated HUVEC monolayers displayed continuous cell–cell adhesion (green fluorescence) and circumferential F-actin lining along the cell junctions (red fluorescence). These features are well in line with previous reports, where the circumferential F-actin linked to the inner membrane domain of transmembrane junction proteins (e.g., VE-cadherin, MUC18) contributes to maintaining the stability of cell junctions.[12,41] Treating HUVEC monolayers with laser irradiation only had a negligible effect on the monolayer morphology. Importantly, treating HUVEC monolayers with AuNRs@MUC18Ab caused a dose-dependent effect on the intercellular gap formation, and the addition of laser treatment after nanorod incubation further exacerbated the gap size and numbers (marked by white triangles, Fig. 3B-3C, S6-S7). Here, visual examination of intercellular gaps was supported by gap area analysis (Fig. 3D), where the treatment of 0.5 nM AuNRs@MUC18Ab plus laser resulted in the most significant gap area (~13 %), in comparison with 0.5 nM AuNRs@MUC18Ab treatment alone (~3%) and the treatment of 0.25 nM AuNRs@MUC18Ab plus laser (~8%). The formation of intercellular gaps was also accompanied by discontinuous cell–cell adhesion, suggesting the disruption of cell junctions and the increase in endothelial permeability. To quantitatively analyze the endothelial permeability, FITC-dextran, a biomolecule labeled with FITC was utilized to mimic molecular anticancer drugs. Through measuring the FITC-dextran transport across endothelial monolayers cultured on a transwell insert, we again noticed the dose-dependent effect of AuNRs@MUC18Ab and the synergistic effect of laser treatment on the endothelial permeability (Fig. 3E), consistent with the gap area data. Among all the treatment groups, 0.5 nM AuNRs@MUC18Ab plus laser led to the highest increase in FITC-dextran transport (3.5-fold increase normalized to untreated group), whereas 0.5 nM AuNRs@MUC18Ab treatment alone and 0.25 nM AuNRs@MUC18Ab plus laser treatment just resulted in a 1.7- and 2.2-fold increase, respectively. Along with the increased gap formation and endothelial permeability, the number and intensity of intracellular F-actin (i.e., stress fibers) was also elevated in a similar trend after the AuNRs@MUC18Ab and laser treatment (Fig. 3F and S8). Given the important role of stress fibers in generating cell contractile forces,[42–45] the upregulation of stress fibers could lead to increased endothelial cell contraction and account for the formation of intercellular gaps. Interestingly, after another 12 h culture in normal growth medium, these newly formed gaps disappeared and the permeabilized endothelial monolayers fully healed (**Figure S9**), suggesting the rapid recoverability of treated endothelium which could be critical to prevent the intravasation of migrating cancer cells to the bloodstream. Together, these results on endothelial monolayers suggest that the AuNRs@MUC18Ab and mild hyperthermia treatment can synergistically enhance the endothelial permeability by causing endothelial cell contraction, disrupting cell junctions, and inducing temporary and recoverable intercellular gaps.

2.4. Enhanced endothelial permeability improves the efficacy of cancer photothermal therapy

Since AuNRs@MUC18Ab and mild hyperthermia treatment increased the transport of molecular drugs (i.e., FITC-dextran experiment) by inducing intercellular gaps, we further investigated if these induced gaps could facilitate the passing of nanorods themselves across the endothelium, considering that the efficacy of photothermal therapy is highly dependent on the accumulation of photo-absorbers into tumor regions.[46–48] Given MUC18 is also over-expressed on many cancer cells, we hypothesized that AuNRs@MUC18Ab, once transiting the tumor endothelium through the induced intercellular gaps, can accumulate in MUC18-positive cancer cells and improve the efficacy of subsequent photothermal ablation of cancer cells. To test this hypothesis, we established an endothelial/cancer cell co-culture model using a transwell system: As shown in Fig. 4A, the confluent HUVEC monolayers were cultured on the top insert and the MUC18-positive cancer cells (MDA-MB-231 cell line from breast cancer or PC3-M cell line from prostate cancer) were grown in the bottom dish. To measure the endothelial permeability for nanorods, the HUVEC monolayers on the top insert were first subjected to different treatments such as AuNRs@MUC18Ab treatment alone and AuNRs@MUC18Ab plus laser treatment to induce intercellular gaps, and then a second batch of AuNRs@MUC18Ab was added to the top insert and measured for their transport to the bottom dish. Similar as the data trend from FITC-dextran transport, the results showed that AuNRs@MUC18Ab and mild hyperthermia treatment on endothelium can also increase the transport of AuNRs@MUC18Ab themselves (Fig. 4B). Significantly, 0.5 nM AuNRs@MUC18Ab alone and 0.5 nM AuNRs@MUC18Ab plus laser treatment on endothelium led to higher AuNRs@MUC18Ab transport across the endothelium (i.e., 1.8- and 2.6-fold increase in transport, normalized to untreated endothelium). Hence, these two treatment groups were used for the subsequent cancer cell experiments.

Following the transport of AuNRs@MUC18Ab, cancer cells in the bottom dish were incubated with the transported nanorods and then subjected to a strong laser irradiation (808 nm, 5 min, 2 W/cm^2) to mimic traditional photothermal therapy. Live-dead cell staining assay was applied to evaluate the efficacy of photothermal ablation of cancer cells. The data revealed that, for both cancer cells, pre-treating endothelium with 0.5 nM AuNRs@MUC18Ab plus laser led to the maximal killing percentage (~65 %) of cancer cells upon photothermal ablation, whereas the 0.5 nM AuNRs@MUC18Ab treatment alone and untreated endothelium resulted in almost no killing effect to cancer cells in the bottom dish (Fig. 4C-4D, S10-S11). Here, it was reassuring to see that 0.5 nM AuNRs@MUC18Ab plus laser treatment on endothelium corresponded to the maximal photothermal ablation of cancer cells because this treatment induced the highest gap area and nanorod transport, as demonstrated earlier (Fig. 3D and 4B). Interestingly, we did not observe significant photothermal ablation of cancer cells in the 0.5 nM AuNRs@MUC18Ab alone group although this treatment caused a 1.8-fold increase in the nanorod transport. To explain this phenomenon, we further looked into the temperature of the cancer cell medium upon strong laser irradiation and found that 0.5 nM AuNRs@MUC18Ab plus laser treatment on endothelium allowed the temperature of cancer cell medium to increase to ~ 42 °C, leading to the thermal ablation of cancer cells, whereas 0.5 nM AuNRs@MUC18Ab treatment alone on endothelium just raised the temperature to ~ 38 °C, due to the insufficient nanorod transport/accumulation to cancer cells (Fig. 4E). Together, these results suggest that AuNRs@MUC18Ab and mild hyperthermia treatment on endothelium can increase the endothelial permeability for AuNRs@MUC18Ab *trans*-endothelial transport, and this pretreatment on endothelium can improve the efficacy of photothermal ablation of cancer cells.

2.5. Understanding mechanism of enhanced endothelial permeability

Finally, we turned our attention to the mechanism by which AuNRs@MUC18Ab and mild hyperthermia enhanced endothelial permeability. Since the increase in stress fibers and cell contractility was observed on the endothelial monolayers, we further asked if these changes on the monolayers stemmed from the morphological change of individual cells. To answer this question, nanomechanical atomic force microscopy (*n*-AFM) and super resolution fluorescence microscopy (SRFM) were utilized to characterize the morphological and cytoskeletal changes of single endothelial cells. Here, *n*-AFM, via scanning through the surface of live cells, can resolve the cytoskeletal structure in the

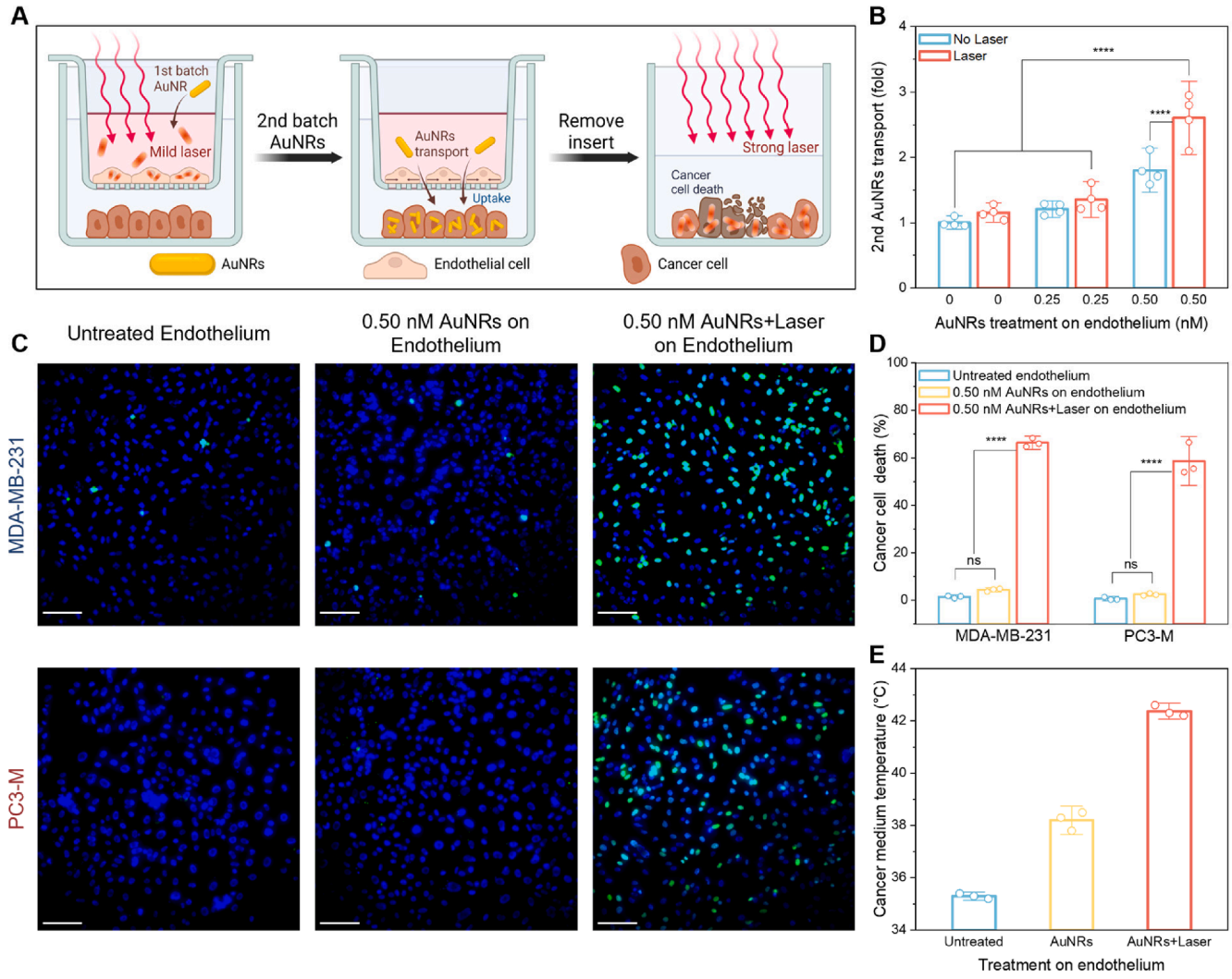

Fig. 4. Enhanced endothelial permeability improves the efficacy of cancer photothermal therapy. (A) Schematic illustrating an endothelial/cancer cell co-culture model is used to evaluate the endothelial permeability for nanorods and subsequent photothermal ablation of cancer cells. AuNRs in Fig. 4 refer to AuNRs@MUC18Ab. (B) Quantification of AuNRs@MUC18Ab transport across the HUVEC monolayers with and without different endothelial treatments. Data are mean ± SD, n = 4. One-way ANOVA with Tukey's post-hoc tests, ****P < 0.0001. (C-D) Live-dead cell staining assay analyzing the efficacy of photothermal ablation of two types of cancer cells in bottom dish of different endothelial-treatment groups. Scale bars: 100 μm. Data are mean ± SD, n = 3. One-way ANOVA with Tukey's post-hoc tests, ****P < 0.0001. (E) Temperature of cancer cell medium in bottom dish after laser irradiation in different endothelial-treatment groups. Data are mean ± SD, n = 3.

dorsal layer of the cell through correlated surface topography and Young's modulus imaging (Fig. 5A), [49,50] while SRFM uses a total internal reflection illumination mode to image the F-actin in the ventral layer of the cell (Fig. 5B).[51,52] As shown in Fig. 5A and S12-S13, the HUVEC, after 0.5 nM AuNRs@MUC18Ab plus laser treatment, changed from a cobblestone- to a spindle-shape morphology, along with the loss of circumferential actin (red arrows) and the formation of stress fibers (green arrows) parallel with the long axis of the cell, suggesting increased contractility of endothelial cells. Fig. 5B and S14-S15 also demonstrated the changed cell shape and dorsal actin cytoskeleton after the treatment, where the improved spatial resolution from SRFM images (versus wide-field microscopy) clearly showed the increased ventral stress fibers and loss of circumferential actin. These visual observations on cell morphology and actin cytoskeleton were further substantiated by the statistical analysis of the images, where the treatment caused the elongated cellular aspect ratio (Fig. 5C), elevated average Young's modulus (Fig. 5D), increased number of stress fibers (Fig. 5E), and altered orientation of F-actin (Fig. 5F) in single cells. Collectively, these imaging results demonstrate that morphological and cytoskeletal changes of single endothelial cells, especially the increase in stress fibers, could account for the cell contraction and the formation of intercellular gaps on the endothelium.

To delve into the molecular mechanism by which AuNRs@MUC18Ab and mild hyperthermia caused the formation of intracellular stress fibers and intercellular gaps on endothelium, we further scrutinized the signaling pathway directly related to the MUC18. Previous studies reveal that MUC18 plays a central role in maintaining the stability of cell–cell adhesion on endothelium by serving as an "anchor" to immobilize the circumferential actin along the inner membrane.[53,54] The inner membrane domain of MUC18 first binds to the phosphorylated ezrin/radixin/moesin protein complex (p-ERM) and further links to the circumferential actin, a protein complex structure necessary to stabilize the cell–cell adhesion (Fig. 5G)[54]. Interestingly, the phosphorylation level of ERM proteins was also proved to corelate with the activation level of RhoA, a common type of GTPase that positively regulates stress fiber formation.[55] Based on these prior findings, we formed our hypothesis for the molecular mechanism: (i) The cell uptake of AuNRs@MUC18Ab will deplete membrane MUC18 into the lysosome degradation pathway, leading to circumferential actin remodeling and instability of cell–cell adhesion (Fig. 5H); and (ii) Following the uptake of nanorods, the mild hyperthermia induced by laser irradiation will upregulate ERM phosphorylation, RhoA activation, and stress fiber

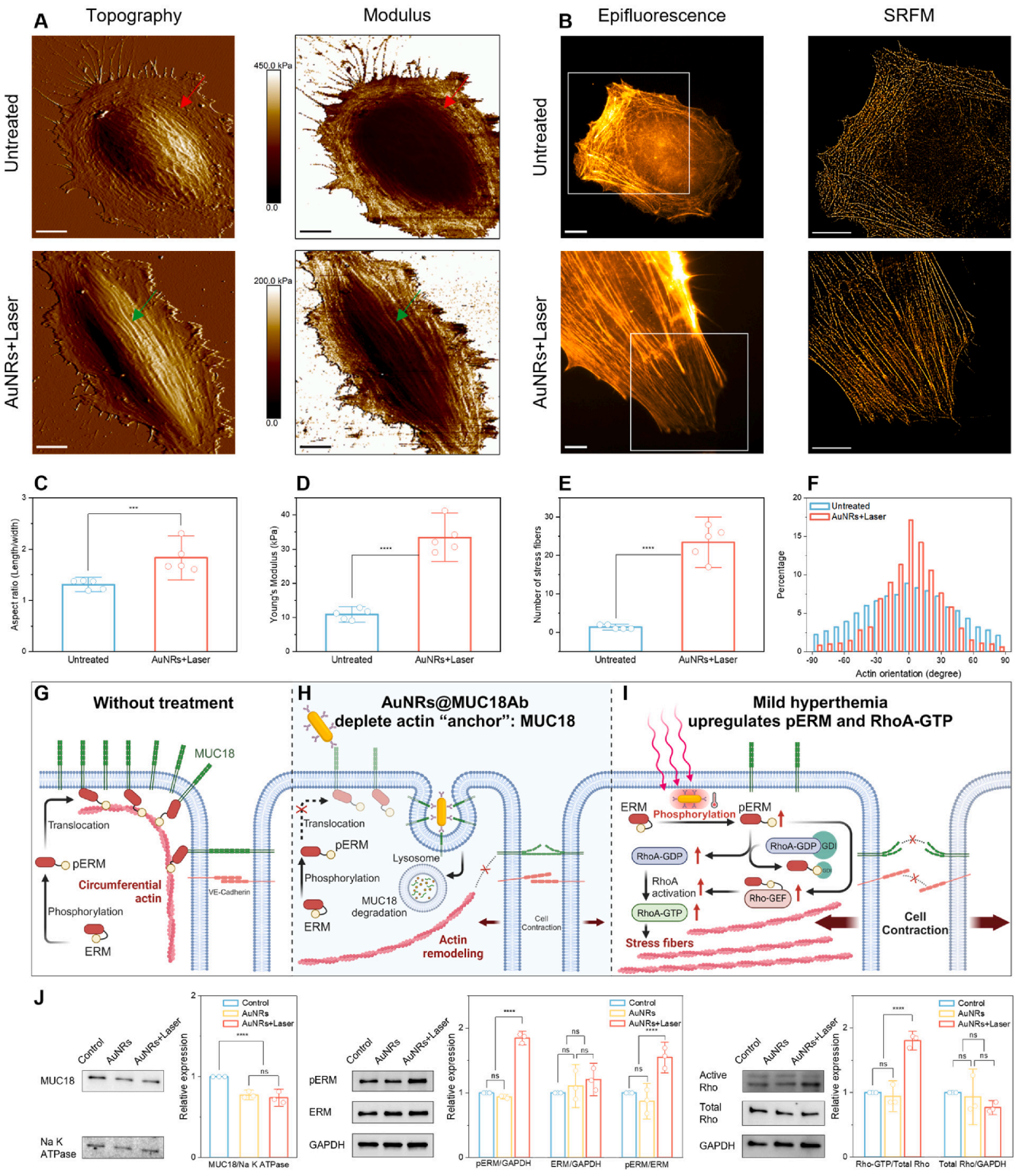

Fig. 5. Mechanism of enhanced endothelial permeability. (A-B) *n*-AFM and SRFM images of single HUVEC with and without the AuNRs@MUC18Ab (abbreviated as AuNRs) plus laser treatment. (C-D) Statistical analysis of cellular aspect ratio and average Young's modulus of HUVEC in different groups from AFM images. (E-F) Quantification of stress fiber number and actin orientation from SRFM images. Scale bars: 10 μm. Data in 5C-5E are mean ± SD, n = 5. Student *t*-test, ***P < 0.001, ****P < 0.0001. (G-I) Schematic illustrating the hypothesis of molecular mechanism of enhanced endothelial permeability. (J) Western blot analysis of the essential proteins in the MUC18 pathway including membrane MUC18, cytoplasmic ERM phosphorylation and RhoA activation. GAPDH and Na/K ATPase are used as housekeeping proteins. Data are mean ± SD, n = 3. One-way ANOVA with Tukey's post-hoc tests, ****P < 0.0001.

formation, further enhancing cell contraction and the formation of intercellular gaps (Fig. 5I).

To validate this hypothesis, Western blotting was performed to quantify the essential proteins in the MUC18 pathway. As presented in Fig. 5J and S16-S18, both AuNRs@MUC18Ab alone and AuNRs@MUC18Ab plus laser treatments caused the decrease of membrane MUC18 to a similar level (~75 %), whereas AuNRs@BSA alone and AuNRs@BSA plus laser treatments were unable to change the MUC18 levels. These suggest that the cell uptake of AuNRs@MUC18Ab could deplete the transmembrane MUC18 and the loss of "anchor" for circumferential actin could lead to the actin remodeling and instability of cell–cell adhesion, as observed earlier and illustrated in Fig. 5H. Considering the tight connection of ERM phosphorylation, RhoA activation, and stress fiber formation,[55] we further quantified p-ERM and RhoA activation levels upon different treatments. The results showed that, among the three experimental groups, only AuNRs@MUC18Ab plus laser treatment upregulated the pERM and RhoA-GTP (~1.8-fold increase compared to untreated and AuNRs@MUC18Ab alone groups). Consistent with previous reports showing the positive effect of mild hyperthermia on the protein phosphorylation, [56–58] the addition of laser treatment following the nanorod uptake upregulated the ERM phosphorylation and RhoA activation. Herein, the upregulated pERM could contribute to the RhoA activation via two simultaneous processes including: (i) binding to Rho GDP-dissociation inhibitor (GDI), which liberates RhoA-GDP for subsequent activation; and (ii) binding to Rho guanine nucleotide exchange factor (Rho-GEF) that accelerates GDP to GTP exchange and facilitates the RhoA activation (as illustrated in Fig. 5I). Collectively, these data demonstrate that AuNRs@MUC18Ab and mild hyperthermia cause the formation of intracellular stress fibers and intercellular gaps on endothelium by depleting membrane MUC18 and upregulating RhoA activation.

3. Conclusions

In summary, we have demonstrated that MUC18-targeted gold nanorods and mild hyperthermia can target MUC18-overexpressed tumor endothelium and enhance its permeability, which improves the efficacy of traditional photothermal therapy and anticancer drug delivery by increasing the transport of photo-absorbers and drugs across the tumor endothelium. The detailed mechanistic studies using AFM, SRFM, and Western blotting suggest that MUC18-targeted gold nanorods and mild hyperthermia synergistically enhance the tumor endothelial permeability by: (i) depleting the membrane MUC18, the "anchor" for circumferential actin, which causes the actin remodeling and loss of cell–cell adhesion; and (ii) upregulating RhoA activation and stress fiber formation, which further increases the cell contractility and intercellular gaps. Considering MUC18 is overexpressed on a variety of tumor endothelium, this approach can be broadly applied to a variety of cancer types, in case their EPR effect is not readily available. Since MUC18 overexpression is also confirmed on the surface of many cancer cells, we expect this approach can be combined with traditional photothermal therapy to treat tumors with non-leaky endothelium. As such, the first step is to enhance tumor endothelial permeability using intravenously injected MUC18-targeted gold nanorods and mild hyperthermia, and the second step is the transport and accumulation of intravenously injected MUC18-targeted gold nanorods to tumor regions, followed by the photothermal ablation of cancer cells. This order can be reversed for the intra-tumoral injected nanorods. Overall, this approach offers a new prospect to improve the efficacy of cancer therapy by actively enhancing the tumor endothelial permeability.

CRediT authorship contribution statement

Xiao Yu: Writing – original draft, Visualization, Methodology, Investigation, Formal analysis, Data curation. **Jinyuan Liu:** Methodology, Investigation, Formal analysis, Data curation. **Aaron Bauer:** Data curation. **Xianqing Wei:** Writing – review & editing, Conceptualization. **Steve Smith:** Writing – review & editing. **Shipeng Ning:** Writing – review & editing, Conceptualization. **Congzhou Wang:** Writing – review & editing, Writing – original draft, Validation, Supervision, Resources, Project administration, Methodology, Investigation, Funding acquisition, Conceptualization.

Declaration of competing interest

The authors declare that they have no known competing financial interests or personal relationships that could have appeared to influence the work reported in this paper.

Data availability

Data will be made available on request.

Acknowledgments

This work is supported by the National Science Foundation CAREER Award (2143972).

Appendix A. Supplementary material

Supplementary data to this article can be found online at https://doi.org/10.1016/j.jcis.2024.07.047.

References

[1] R.S. Riley, C.H. June, R. Langer, M.J. Mitchell, Delivery technologies for cancer immunotherapy, Nat. Rev. Drug Discov. 18 (2019) 175–196.
[2] H. Maeda, J. Wu, T. Sawa, Y. Matsumura, K. Hori, Tumor vascular permeability and the epr effect in macromolecular therapeutics: a review, J. Control. Release 65 (2000) 271–284.
[3] X. Li, Y. Gao, H. Li, J.-P. Majoral, X. Shi, A. Pich, Smart and bioinspired systems for overcoming biological barriers and enhancing disease theranostics, Prog. Mater Sci. 140 (2023) 101170.
[4] M.I. Setyawati, C.Y. Tay, D. Docter, R.H. Stauber, D.T. Leong, Understanding and exploiting nanoparticles' intimacy with the blood vessel and blood, Chem. Soc. Rev. 44 (2015) 8174–8199.
[5] C. Song, Z. Ouyang, H. Guo, J. Qu, Y. Gao, J. Xia, M. Shen, X. Shi, Core-Shell tecto dendrimers enable enhanced tumor MR imaging through an amplified Epr effect, Biomacromolecules 22 (2021) 2181–2188.
[6] X. Xu, T. Xiao, C. Zhang, Z. Wang, G. Li, J. Chen, Z. Ouyang, H. Wang, X. Shi, M. Shen, Multifunctional low-generation dendrimer nanogels as an emerging probe for tumor-specific Ct/Mr dual-modal imaging, Biomacromolecules 24 (2023) 967–976.
[7] N. Ni, W. Wang, Y. Sun, X. Sun, D.T. Leong, Inducible endothelial leakiness in nanotherapeutic applications, Biomaterials 287 (2022) 121640.
[8] F. Chen, W. Cai, Tumor vasculature targeting: a generally applicable approach for functionalized nanomaterials, Small 10 (2014) 1887–1893.
[9] L. Zhao, W. Yuan, J. Li, L. Yang, Y. Su, J. Peng, R. Chen, H.P. Tham, H. Chen, W. Q. Lim, H. Xiang, P. Xing, F. Li, Y. Zhao, Independent of Epr effect: a smart delivery nanosystem for tracking and treatment of nonvascularized intra-abdominal metastases, Adv. Funct. Mater. 28 (2018) 1806162.
[10] X. Liu, J. Jiang, H. Meng, Transcytosis - an effective targeting strategy that is complementary to "Epr Effect" for pancreatic cancer nano drug delivery, Theranostics 9 (2019) 8018–8025.
[11] S.K. Golombek, J.-N. May, B. Theek, L. Appold, N. Drude, F. Kiessling, T. Lammers, Tumor targeting Via Epr: strategies to enhance patient responses, Adv. Drug Deliv. Rev. 130 (2018) 17–38.
[12] J. Wu, Z. Zhu, W. Liu, Y. Zhang, Y. Kang, J. Liu, C. Hu, R. Wang, M. Zhang, L. Chen, L. Shao, How nanoparticles open the paracellular route of biological barriers: mechanisms, applications, and prospects, ACS Nano 16 (2022) 15627–15652.
[13] A.L.B. Seynhaeve, M. Amin, D. Haemmerich, G.C. van Rhoon, T.L.M. ten Hagen, Hyperthermia and smart drug delivery systems for solid tumor therapy, Adv. Drug Deliv. Rev. 163–164 (2020) 125–144.
[14] L. Duan, L. Yang, J. Jin, F. Yang, D. Liu, K. Hu, Q. Wang, Y. Yue, N. Gu, Micro/nano-bubble-assisted ultrasound to enhance the Epr effect and potential theranostic applications, Theranostics 10 (2020) 462–483.
[15] K.T. Butterworth, S.J. McMahon, F.J. Currell, K.M. Prise, Physical basis and biological mechanisms of gold nanoparticle radiosensitization, Nanoscale 4 (2012) 4830–4838.
[16] Z.-Q. Zuo, K.-G. Chen, X.-Y. Yu, G. Zhao, S. Shen, Z.-T. Cao, Y.-L. Luo, Y.-C. Wang, J. Wang, Promoting tumor penetration of nanoparticles for cancer stem cell therapy by Tgf-B signaling pathway inhibition, Biomaterials 82 (2016) 48–59.

[17] A.J. Gormley, N. Larson, S. Sadekar, R. Robinson, A. Ray, H. Ghandehari, Guided delivery of polymer therapeutics using plasmonic photothermal therapy, Nano Today 7 (2012) 158–167.
[18] Z. Zhang, J. Wang, X. Nie, T. Wen, Y. Ji, X. Wu, Y. Zhao, C. Chen, Near infrared laser-induced targeted cancer therapy using thermoresponsive polymer encapsulated gold nanorods, J. Am. Chem. Soc. 136 (2014) 7317–7326.
[19] B. St Croix, C. Rago, V. Velculescu, G. Traverso, K.E. Romans, E. Montgomery, A. Lal, G.J. Riggins, C. Lengauer, B. Vogelstein, K.W. Kinzler, Genes expressed in human tumor endothelium, Science 289 (2000) 1197–1202.
[20] S. Thomann, T. Longerich, A.V. Bazhin, W. Mier, P. Schemmer, E. Ryschich, Selective targeting of liver cancer with the endothelial marker Cd146, Oncotarget 5 (2014) 8614–8624.
[21] X. Chen, H. Yan, D. Liu, Q. Xu, H. Duan, J. Feng, X. Yan, C. Xie, Structure Basis for Aa98 Inhibition on the Activation of Endothelial Cells Mediated by Cd146, iScience 24 (2021) 102417.
[22] Z. Wang, Q. Xu, N. Zhang, X. Du, G. Xu, X. Yan, Cd146, from a melanoma cell adhesion molecule to a signaling receptor, Signal Transduct. Target. Ther. 5 (2020) 148.
[23] B. Nikoobakht, M.A. El-Sayed, Preparation and growth mechanism of gold nanorods (Nrs) using seed-mediated growth method, Chem. Mater. 15 (2003) 1957–1962.
[24] T.K. Sau, C.J. Murphy, Seeded high yield synthesis of short Au nanorods in aqueous solution, Langmuir 20 (2004) 6414–6420.
[25] N.R. Jana, L. Gearheart, C.J. Murphy, Seed-mediated growth approach for shape-controlled synthesis of spheroidal and rod-like gold nanoparticles using a surfactant template, Adv. Mater. 13 (2001) 1389–1393.
[26] M. Tebbe, C. Kuttner, M. Männel, A. Fery, M. Chanana, Colloidally stable and surfactant-free protein-coated gold nanorods in biological media, ACS Appl. Mater. Interfaces 7 (2015) 5984–5991.
[27] A.S.D.S. Indrasekara, R.C. Wadams, L. Fabris, Ligand exchange on gold nanorods: going back to the future, Part. Part. Syst. Char. 31 (2014) 819–838.
[28] J. Liu, L. Kang, S. Smith, C. Wang, Transmembrane Muc18 targeted polydopamine nanoparticles and a mild photothermal effect synergistically disrupt actin cytoskeleton and migration of cancer cells, Nano Lett. 21 (2021) 9609–9618.
[29] Z. Wang, J. Luan, A. Seth, L. Liu, M. You, P. Gupta, P. Rathi, Y. Wang, S. Cao, Q. Jiang, X. Zhang, R. Gupta, Q. Zhou, J.J. Morrissey, E.L. Scheller, J.S. Rudra, S. Singamaneni, Microneedle patch for the ultrasensitive quantification of protein biomarkers in interstitial fluid, Nat. Biomed. Eng. 5 (2021) 64–76.
[30] J. Liu, S. Smith, C. Wang, Photothermal attenuation of cancer cell stemness, chemoresistance, and migration using Cd44-targeted Mos2 nanosheets, Nano Lett. 23 (2023) 1989–1999.
[31] S.M. Bhat, V.A. Badiger, S. Vasishta, J. Chakraborty, S. Prasad, S. Ghosh, M. B. Joshi, 3d tumor angiogenesis models: recent advances and challenges, J Cancer Res Clin Oncol 147 (2021) 3477–3494.
[32] M.R. Richardson, X. Lai, F.A. Witzmann, M.C. Yoder, Venous and arterial endothelial proteomics: mining for markers and mechanisms of endothelial diversity, Expert Rev Proteomics 7 (2010) 823–831.
[33] J. Liu, S. Smith, C. Wang, Reversing the epithelial-mesenchymal transition in metastatic cancer cells using Cd146-targeted black phosphorus nanosheets and a mild photothermal treatment, ACS Nano 16 (2022) 3208–3220.
[34] J.D. Martin, G. Seano, R.K. Jain, Normalizing function of tumor vessels: progress, opportunities, and challenges, Annu. Rev. Physiol. 81 (2019) 505–534.
[35] L. Zhao, X. Zhang, X. Wang, X. Guan, W. Zhang, J. Ma, Recent advances in selective photothermal therapy of tumor, J. Nanobiotechnol. 19 (2021) 1–15.
[36] Z. Li, Y. Zhu, Z. Zhang, H. Wang, C. Wang, C. Xu, S. Li, S. Zhang, X. Yang, Z. Li. Softness-aided mild hyperthermia boosts stiff nanomedicine by regulating tumor mechanics. Adv. Sci. *n/a*, 2306730.
[37] C. Wang, H. Wang, H. Yang, C. Xu, Q. Wang, Z. Li, Z. Zhang, J. Guan, X. Yu, X. Yang, X. Yang, Z. Li, Targeting cancer-associated fibroblasts with hydroxyethyl starch nanomedicine boosts cancer therapy, Nano Res. 16 (2023) 7323–7336.
[38] C. Wang, Q. Wang, H. Wang, Z. Li, J. Chen, Z. Zhang, H. Zeng, X. Yu, X. Yang, X. Yang, Z. Li, Hydroxyethyl starch-folic acid conjugates stabilized theranostic nanoparticles for cancer therapy, J. Control. Release 353 (2023) 391–410.
[39] Y. Xiong, W. Wang, Q. Deng, Z. Zhang, Q. Wang, Z. Yong, C. Sun, X. Yang, Z. Li, Mild photothermal therapy boosts nanomedicine antitumor efficacy by disrupting DNA damage repair pathways and modulating tumor mechanics, Nano Today 49 (2023) 101767.
[40] X. Huang, I.H. El-Sayed, W. Qian, M.A. El-Sayed, Cancer cell imaging and photothermal therapy in the near-infrared region by using gold nanorods, J. Am. Chem. Soc. 128 (2006) 2115–2120.
[41] J. Liu, X. Yu, A. Braucht, S. Smith, C. Wang, N-cadherin targeted melanin nanoparticles reverse the endothelial-mesenchymal transition in vascular endothelial cells to potentially slow the progression of atherosclerosis and cancer, ACS Nano 18 (2024) 8229–8247.
[42] L. Lu, Y. Feng, W.J. Hucker, S.J. Oswald, G.D. Longmore, F.C. Yin, Actin stress fiber pre-extension in human aortic endothelial cells, Cell Motil Cytoskeleton 65 (2008) 281–294.
[43] M. Wang, B. Cheng, Y. Yang, H. Liu, G. Huang, L. Han, F. Li, F. Xu, Microchannel stiffness and confinement jointly induce the mesenchymal-amoeboid transition of cancer cell migration, Nano Lett. 19 (2019) 5949–5958.
[44] J. Escribano, M.B. Chen, E. Moeendarbary, X. Cao, V. Shenoy, J.M. Garcia-Aznar, R.D. Kamm, F. Spill, Balance of mechanical forces drives endothelial gap formation and may facilitate cancer and immune-cell extravasation, PLoS Comput. Biol. 15 (2019) e1006395.
[45] G. Huang, F. Xu, G.M. Genin, T.J. Lu, Mechanical microenvironments of living cells: a critical frontier in mechanobiology, Acta Mech. Sin. 35 (2019) 265–269.
[46] A. Seth, H. Gholami Derami, P. Gupta, Z. Wang, P. Rathi, R. Gupta, T. Cao, J. J. Morrissey, S. Singamaneni, Polydopamine-mesoporous silica core-shell nanoparticles for combined photothermal immunotherapy, ACS Appl. Mater. Interfaces 12 (2020) 42499–42510.
[47] S. Huang, Y. Ye, C. Jiang, R. Wang, W. Hu, S. Raza, J. Ouyang, Y. Pan, J. Liu, Current and promising applications of mofs loaded with ptas on photothermal therapy, React. Funct. Polym. 193 (2023) 105743.
[48] J.-Q. Liu, M. Li, Z. Zhang, Y. Yu, H. Yuan, A. Nezamzadeh-Ejhieh, Y. Pan, Q. Lan, Recent Advances of Zn-Mofs and their derivatives for cancer therapeutic applications, Mater. Adv. (2023).
[49] A. Calzado-Martín, M. Encinar, J. Tamayo, M. Calleja, A. San Paulo, Effect of actin organization on the stiffness of living breast cancer cells revealed by peak-force modulation atomic force microscopy, ACS Nano 10 (2016) 3365–3374.
[50] A.C. Dumitru, M.A. Poncin, L. Conrard, Y.F. Dufrêne, D. Tyteca, D. Alsteens, Nanoscale membrane architecture of healthy and pathological red blood cells, Nanoscale Horiz. 3 (2018) 293–304.
[51] S. van de Linde, A. Löschberger, T. Klein, M. Heidbreder, S. Wolter, M. Heilemann, M. Sauer, Direct stochastic optical reconstruction microscopy with standard fluorescent probes, Nat. Protoc. 6 (2011) 991–1009.
[52] G.T. Dempsey, J.C. Vaughan, K.H. Chen, M. Bates, X. Zhuang, Evaluation of fluorophores for optimal performance in localization-based super-resolution imaging, Nat. Methods 8 (2011) 1027–1036.
[53] N. Bardin, F. Anfosso, J.M. Massé, E. Cramer, F. Sabatier, A. Le Bivic, J. Sampol, F. Dignat-George, Identification of Cd146 as a component of the endothelial junction involved in the control of cell-cell cohesion, Blood 98 (2001) 3677–3684.
[54] Y. Luo, C. Zheng, J. Zhang, D. Lu, J. Zhuang, S. Xing, J. Feng, D. Yang, X. Yan, Recognition of Cd146 as an Erm-binding protein offers novel mechanisms for melanoma cell migration, Oncogene 31 (2012) 306–321.
[55] K. Kawaguchi, S. Yoshida, R. Hatano, S. Asano, Pathophysiological roles of Ezrin/Radixin/Moesin proteins, Biol. Pharm. Bull. 40 (2017) 381–390.
[56] Y. Wu, M.R.K. Ali, B. Dong, T. Han, K. Chen, J. Chen, Y. Tang, N. Fang, F. Wang, M. A. El-Sayed, Gold nanorod photothermal therapy alters cell junctions and actin network in inhibiting cancer cell collective migration, ACS Nano 12 (2018) 9279–9290.
[57] R.F. Duncan, J.W. Hershey, Protein synthesis and protein phosphorylation during heat stress, recovery, and adaptation, J Cell Biol 109 (1989) 1467–1481.
[58] H.S. Han, M. Karabiyikoglu, S. Kelly, R.A. Sobel, M.A. Yenari, Mild hypothermia inhibits nuclear factor-kappab translocation in experimental stroke, J Cereb Blood Flow Metab 23 (2003) 589–598.